AUT Journal of Mechanical Engineering

AUT J. Mech. Eng., 7(1) (2023) 41-50
DOI: 10.22060/ajme.2023.21665.6042

Simultaneous impacts of acoustic and inertial forces on the separation of microparticles

Z. Taheri, M. Bayareh*, B. Ghasemi, M. Nazemi Ashani

Department of Mechanical Engineering, Shahrekord University, Shahrekord, Iran

ABSTRACT: The isolation of microparticles plays a crucial role in various applications, including biological and medical sciences. In this paper, the separation of polystyrene (PS) and polymethyl methacrylate (PMMA) particles suspended in water is simulated using the acoustic field and channel geometry. The microchannel consists of two parts, a curve-shaped and a straight part. Passive separation occurs in the curve-shaped section due to the flow rotation in the microchannel, and the acoustic force acts and enhances the separation efficiency in the straight part. The acoustic field is created by a pair of aluminum transducers on a piezoelectric substrate. In this study, firstly, the separation of microparticles is done using a microchannel without an acoustic field, leading to a separation efficiency of 81%. The acoustic force is then applied to the microchannel and, the maximum separation efficiency of 94% is obtained. It is observed that the separation efficiency is directly related to the frequency of the acoustic field and inversely related to the inlet flow rate. It should be noted that there is an optimal value for the applied frequency due to the specific value of the channel width. Also, the amount of separation efficiency is improved by enhancing the inlet power. It is observed that as the distance between transducers and microchannels is enhanced, the separation efficiency is reduced.

Review History:

Received: Aug. 06, 2022
Revised: Jan. 27, 2023
Accepted: Mar. 03, 2023
Available Online: Mar. 03, 2023

Keywords:

Microfluidics
Acoustic field
Passive separation
Active separation

1- Introduction

In recent years, microfluidic devices have been broadly utilized due to their low cost, low energy consumption, and compatibility with the environment, especially in biological applications [1-4]. The use of these devices in chemical applications [5], interdisciplinary sciences [6], and biological and medical sciences [7] has been increased rapidly. These devices are divided into two categories: active devices and passive ones. In passive devices, the inertial force applied to the particles, as well as fluid and particle interaction results in the separation of microparticles relying on microchannel geometry [8]. The use of inertia force and Dean flow [9-10], pinch flow fractionation filtration [11-12], and placement of obstacles in the microchannel are among the passive separation methods. Devices that use external actuators to improve separation efficiency are known as active microfluidic devices. One of the external forces used in microfluidic devices is acoustic force. Compatibility with the environment, especially the biological environment, has made the use of this force reasonable. The interaction between an electric current and a piezoelectric substrate is utilized to create sound waves [13]. Sound waves are divided into three categories: static sound waves, dynamic sound waves, and volumetric ones. In standing acoustic waves, the microchannel is located between two pairs of transducers [14]. As a result of the collision of two acoustic waves that are propagating in opposite directions, a stationary acoustic wave is created. In dynamic acoustic waves, the transducer pair is placed on one side of the microchannel [15]. Volumetric waves are applied in the microchannel volume [16].

Extensive studies have been conducted in the field of applying the acoustic field to separate microparticles/cells. Nama *et al.* [17] calculated the acoustic radiation force applied to suspended particles using two-dimensional numerical simulations. They simplified the system by using a piezoelectric substrate instead of modeling it as a separate domain. As a result, the energy dissipation was not accurately modeled because neither this domain was included in the simulation nor the impedance boundary conditions applied to the microchannel walls. Hsu *et al.* [18] examined the application of dual-wavelength standing surface acoustic waves to control the migration of particles inside the microchannel. Ma *et al.* [19] found a single-actuator bandpass filtration to sort particles with small and large diameters. The bandpass filtration scaled strongly with nonlinear force in the regime where particle diameters were on the wavelength scale or larger. They separated 15.2 μm polystyrene particles from 10.2 and 19.5 μm ones, as well as 10.2 μm particles from 8 and 11.8 μm particles. Han *et al.* [20] developed an acoustofluidic platform based on standing surface acoustic waves and analyzed the effect of droplet contact angle. They showed that frequency, power, and particle diameter are effective

*Corresponding author's email: m.bayareh@sku.ac.ir

on the contact angle of the drop. In addition, they explained the reason for the position of suspended particles in droplets and the mechanism of particle separation. They employed a standing surface acoustic wave to achieve a permanent effect on one or two types of suspended particles in a drop. Nguyen *et al.* [21] developed an acoustofluidic closed-loop control system in which standing surface acoustic waves were used to control the selective, automatic, and precise position of a cell or microparticle in a microfluidic chamber. Lei *et al.* [22] presented a continuous flow-based two-stage acoustic microparticle separation with a fluid model consisting of three main parts: the acoustic focusing zone, the transition zone, and the acoustic separation zone. The acoustophoresis applied to the microparticles of different sizes in the channel was modeled based on Newton's second law, where acoustic radiation and drag forces were considered. They found that an acoustic focusing process with a suitable force range can concentrate all particles before entering the separation zone and improve the separation efficiency.

The literature review demonstrates that the acoustophoresis can be applied to isolate different sizes of microparticles due to the application of acoustic radiation and drag forces. Besides, microparticles may be separated by using the specific geometry of the microchannel to utilize inertial force. In the present work, the separation of PS and PMMA particles suspended in water is simulated by applying an acoustic field. The inertial effect is effective in the curved section and the acoustic field is applied in the straight part. In other words, passive separation occurs in the curved part due to the rotation of the flow in the microchannel, and active separation is employed in the straight part. The combination of passive and active techniques is utilized to improve the separation efficiency.

2- Governing Equations

The application of acoustic waves in the fluid causes the creation of the acoustic radiation force. If the diameter of the suspended particles in the fluid is less than half the wavelength of the acoustic wave, they are affected by this force. Newton's second law for the force and velocity of particles is as follows [22]:

$$\mathbf{F} = m_p \frac{d\mathbf{u}_p}{dt} \tag{1}$$

where $\mathbf{F}$, m_p, $\mathbf{u}_p$ and t are the force, particle mass, particle velocity, and time, respectively. The radiation force includes drag force ($\mathbf{F}_D$) and acoustic radiation force ($\mathbf{F}_{Rad}$). For spherical particles moving in a fluid with the velocity of $\mathbf{u}_f$, the drag force is [23-24].

$$\mathbf{F}_D = -3\pi\mu d\left(\mathbf{u}_p - \mathbf{u}_f\right) \tag{2}$$

Assuming an incompressible fluid and ignoring the gravity force, the momentum equation is as follows:

$$\rho_f \frac{d\mathbf{u}_f}{dt} = -\nabla p + \mu\nabla^2\mathbf{u}_f \tag{3}$$

For spherical particles, the acoustic radiation force is [25].

$$\mathbf{F}_{Rad} = -\nabla U_{Rad} \tag{4}$$

where U_{Rad} is the acoustic potential energy:

$$U_{Rad} = \frac{\pi}{6}d^3\left(\frac{f_1}{2\rho c_f^2}\overline{p^2} - \frac{3f_2}{4}\rho\overline{\mathbf{u}_l^2}\right) \tag{5}$$

where

$$f_1 = 1 - \frac{k_p}{k_f} \tag{6}$$

$$f_2 = \frac{2\left(\rho - \rho_f\right)}{2\rho + \rho_f} \tag{7}$$

Here, ρ, p, k_f, k_p, c_f, and ρ_f are particle density, acoustic field pressure, fluid compressibility, particle compressibility, acoustic velocity in the fluid, and fluid density, respectively. $\overline{p^2}$ and $\overline{u^2}$ represent the average values of the square of pressure and inlet velocity, respectively. The direction of particles motion depends on the sign of acoustic field contrast ($\phi\left(\beta,\rho\right)$) which is defined as follows [16].

$$\phi\left(\beta,\rho\right) = \frac{5\rho - 2\rho_f}{2\rho + \rho_f} - \frac{k_p}{k_f} \tag{8}$$

The positive sign of $\phi\left(\beta,\rho\right)$ causes the particles to move toward pressure nodes and its negative sign causes the particles to move toward pressure antinodes. For PM and PMMA particles that are examined in this study, this parameter is equal to -0.28 and 1.16, respectively. Therefore, PM particles move toward pressure nodes and PMMA particles move toward pressure antinodes.

The Helmholtz equation is solved to calculate $\overline{p^2}$ and $\overline{u^2}$. Acoustic waves are produced by piezoelectric due to the interaction of the piezoelectric substrate and the electric current applied by the aluminum electrodes. Therefore, the

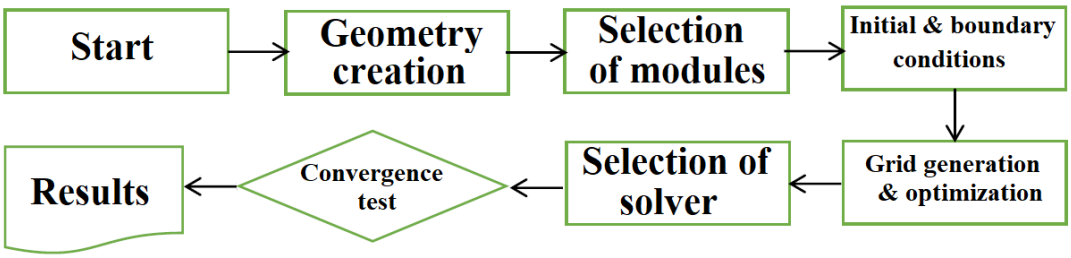

Fig. 1. Modeling flowchart to simulate the present problem.

linear piezoelectric equations must be solved:

$$\mathbf{S} = \mathbf{s}_E T + \mathbf{e}^t \mathbf{E} \tag{9}$$

(10)

Here, $\mathbf{s}_E$, ε_r, ε_0, $\mathbf{E}$, T, $\mathbf{S}$, $\mathbf{D}$, and $\mathbf{e}$ represent the compliance matrix, relative permeability matrix, vacuum permeability, electric field, stress, charge transfer density, and piezoelectric matrix, respectively. $\mathbf{e}^t$ is the transpose of the matrix *e*. Also, the applied acoustic field pressure is obtained as follows [26]:

$$p = \sqrt{\frac{Pz}{A}} \tag{11}$$

where $Z = \rho_f \times c_f$ is the impedance of the acoustic field and A is the area of the area where the acoustic wave is applied. In this study, the reference distance between the transducers and the microchannel wall is equal to half of the applied wavelength, i.e. 75 μm. This amount of distance causes a pressure node to form in the middle of the microchannel.

Navier-Stokes equations are solved using the finite element method by employing COMSOL Multiphysics software. Also, the P3+P2 scheme is utilized to solve the velocity and pressure fields. This scheme means third-order elements and second-order elements for velocity components and pressure field, respectively. The time step is 10^{-3} s and the convergence criterion is 10^{-6}. The Generalized Minimal Residual (GMRES) iterative solver is employed to solve the model. The GMRES solver generates a sequence of orthogonal vectors for asymmetric systems and the residual norm is computed with minimum iteration at every step. Fig. 1 demonstrates the modeling flowchart.

3- Problem Description and Grid Study

The geometry of the present study, as shown in Fig. 2, includes three parts: spiral channel, straight channel, and transducers. First, the particles enter the spiral section of the microchannel with a curvature of about 270° and are partially separated due to the centrifugal force based on their mass and density. Then, the particles enter the straight part of the microchannel, which is placed between the pair of aluminum transducers. The width of the microchannel in the spiral and straight sections is 150 μm. The characteristics of the microparticles and fluid are presented in Table 1.

The microchannel has three outlets and the substrate placed under the microchannel is Polydimethylsiloxane (PDMS) which is $LiNbO_3$. 1.5V voltage is applied to the transducers to produce the acoustic wave. The sample entering the microchannel has a uniform velocity of 10^{-4} m/s, i.e., creeping flow regime, and the no-slip boundary condition is imposed on the walls.

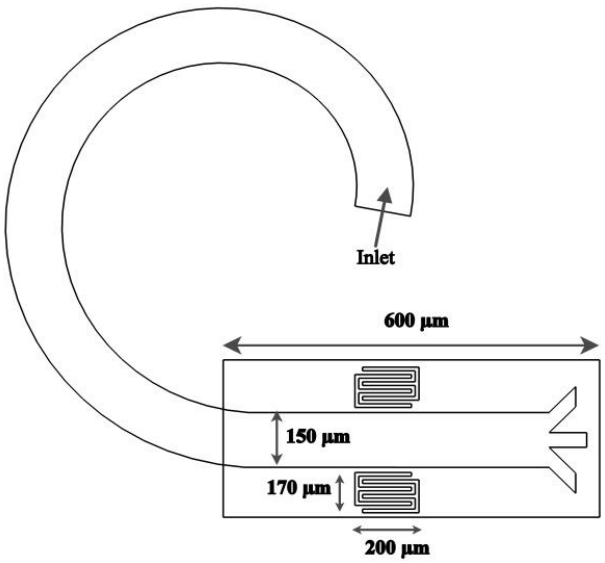

Fig. 2. Schematic of the present problem.

Table 1. Characteristic of fluid and microparticles [4].

Property	PS	PMMA	Fluid
Diameter, μm	10	15	_
Density, kg/m^3	1050	1180	998
Sound speed, m/s	1260	2757	1481
Shear wave speed, m/s	1120	1400	-
Compressibility, Pa^{-1}	6.0×10^{-10}	1.3×10^{-12}	4.5×10^{-10}

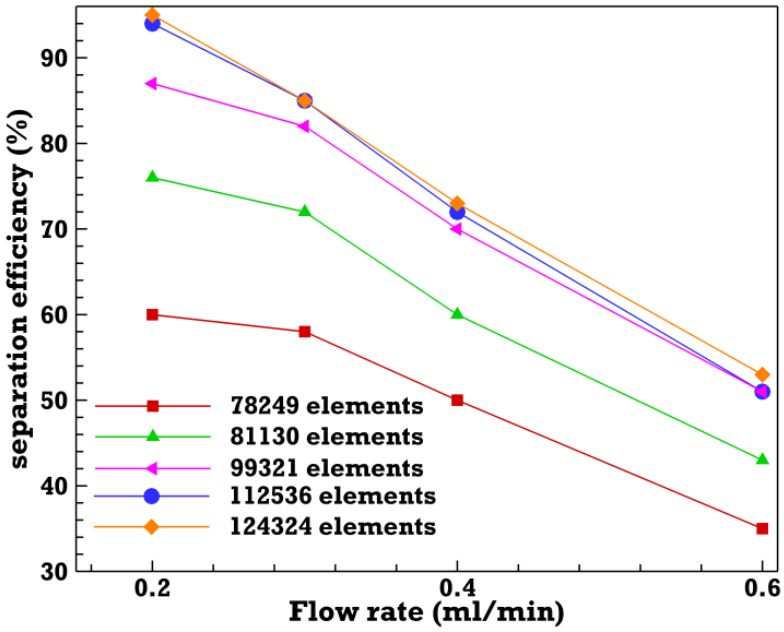

Fig. 3. Separateion efficiency in terms of mass flow rate for different grid resolutions when the frequency is 5 MHz.

Several grids with different elements are generated to perform a grid study. Fig. 3 illustrates the changes in the separation efficiency in terms of the inlet flow rate. It is observed that there is no noticeable change in the separation efficiency by changing the number of elements from 112536 to 124324. Thus, the grid with 112536 elements is selected for further simulations (Fig. 4). The values of y^+ are placed in the range of $10 < y^+ < 150$ in the current simulations to obtain precise results. It should be noted that the standard logarithmic law can be utilized when $30 < y^+ < 300$.

4- Validation

To verify the present numerical simulations, the present results are compared with those reported by Petersson et al. [27] (Fig. 5A) and Nazemi et al. [4] (Fig. 5B). These figures demonstrate the separation efficiency for various inlet mass flow rates and different input powers, indicating excellent agreement of the present simulations with the two other works. In both comparisons, the maximum error between the results obtained from the present work and other numerical simulations is less than 5%.

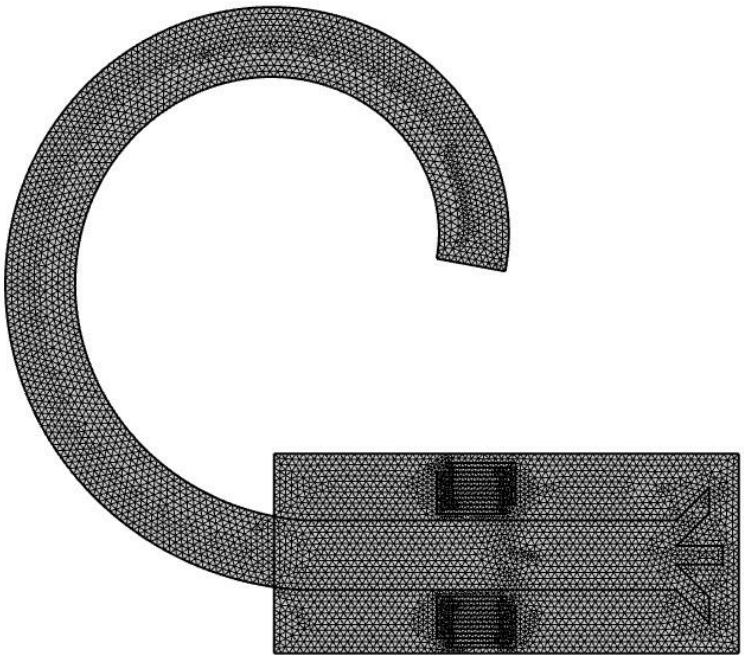

Fig. 4. The grid generated on the present problem.

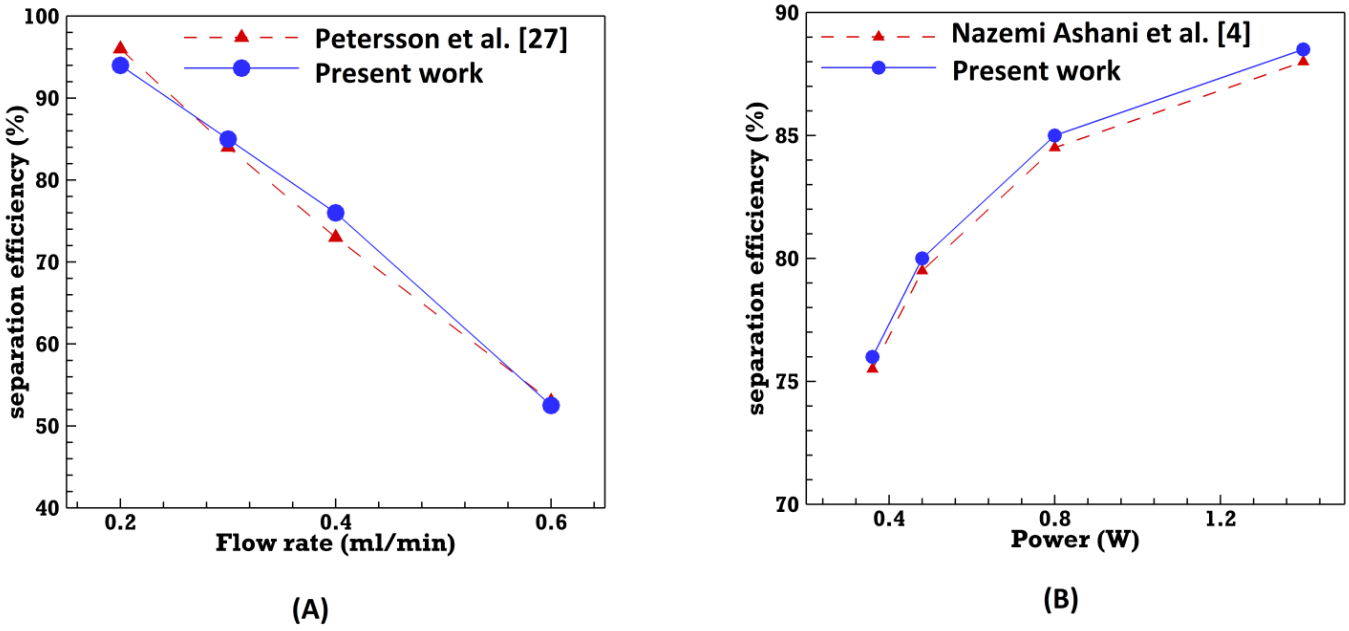

Fig. 5. Separation efficiency in terms of (A) flow rate, and (B) input power.

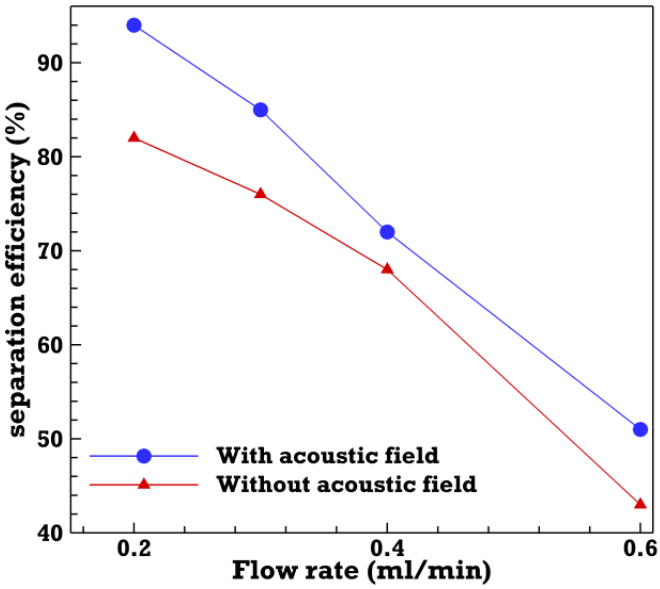

Fig. 6. The effect of applying the acoustic field on the separation efficiency for the frequency of 5 MHz, the input power of 1.4 W, and the wall thickness of 10 µm.

5- Results

If the acoustic field is not applied to the microchannel, the acoustic radiation force is not generated. Therefore, it is expected that the separation efficiency when the acoustic field is applied will be lower than that in the absence of the acoustic field. Fig. 6 demonstrates the changes in the separation efficiency compared in terms of the inlet flow rate with and without an acoustic field. This separation efficiency is calculated for the frequency of 5 MHz, the input power of 1.4 *W*, and the wall thickness of 10 μm. For both cases, the decreasing trend of the separation efficiency changes with the flow rate is almost the same. It can be concluded that as the flow rate is enhanced, the separation efficiency is reduced with almost the same slope with and without the acoustic field. However, the separation efficiency is much higher when the acoustic field is applied due to the major role of acoustic radiation force applied to the microparticles. For instance, for the flow rate is 0.2 *ml/min*, the separation efficiency is enhanced by about 14.6% when the acoustic field is applied to the microchannel compared to the case without applying the acoustic field.

5- 1- Effect of input power

Fig. 7 depicts the separation efficiency for different values of input power when the applied frequency is 5 *MHz*. It is observed that the separation efficiency is enhanced with the input power. According to Eq. 11, the amount of acoustic field pressure is intensified by increasing the input power, resulting in an increment in the acoustic radiation force. This force causes particles to move toward pressure nodes and antinodes. As a result, the deviation of the particles, i.e. their lateral distance, is enhanced and the separation efficiency is improved. For example, by increasing the input power from about 0.4 *W* to 1.4 *W*, the separation efficiency is enhanced by about 20%.

5- 2- Effect of inlet flow rate

When the flow rate entering the microchannel is enhanced, the flow velocity is increased. In this case, the microparticles suspended in the fluid are exposed to acoustic waves for a shorter time and a smaller acoustic radiation force is applied to them. To examine the impact of the inlet flow rate, the mass flow rate changes from 0.2 *ml/min* to 0.6 *ml/min* when the applied frequency is 5 *MHz* and input power is 1.4 *W*. Fig. 8 demonstrates that the separation efficiency is reduced from 94% to 51% when the inlet flow rate is enhanced from 0.2 *ml/min* to 0.6 *ml/min*. The maximum separation efficiency corresponds to a flow rate of 0.2 *ml/min* and the minimum one is related to 0.6 *ml/min*.

5- 3- Effect of applied frequency

Fig. 9 reveals the variations of the separation efficiency by changing the applied frequency. Since the wavelength λ is proportional to the applied frequency, $\lambda = c_f/f$, an increment in the frequency results in a reduction in the wavelength, leading to the change of the pressure nodes and antinodes in the channel cross-sections. Enhancing the frequency causes the formation of more pressure nodes and a higher migration rate of microparticles. As a result, the separation efficiency is improved. It is worth noting that there is an optimal frequency, in which the separation efficiency is maximal. Contrary to the impact of input power and inlet flow rate, an increment in the applied frequency may lead to a reduction in the separation efficiency. Even though the number of pressure nodes and antinodes is increased with the frequency, the channel width is a limitation for the amount of the deviation of microparticles. Here, the width of the microchannel is 150 μm and it is not sufficient to support the higher deviations of PS and PMMA particles.

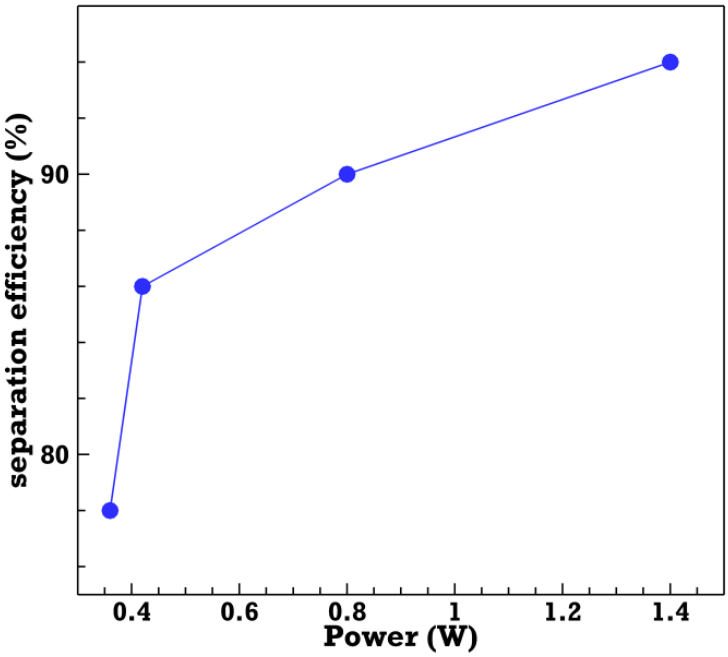

Fig. 7. Separation efficiency versus input power when the applied frequency is 5 MHz and the flow rate is 0.2 µl/min.

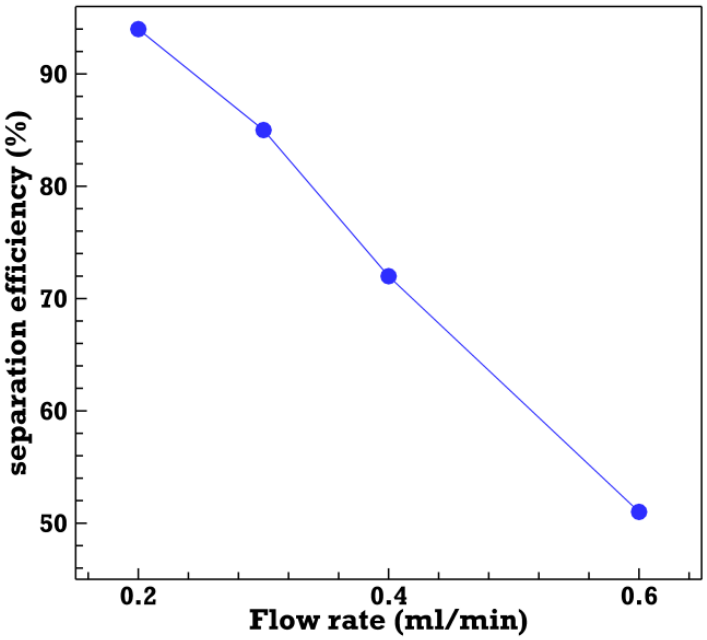

Fig. 8. Separation efficiency versus inlet flow rate when the applied frequency is 5 MHz and input power is 1.4 W.

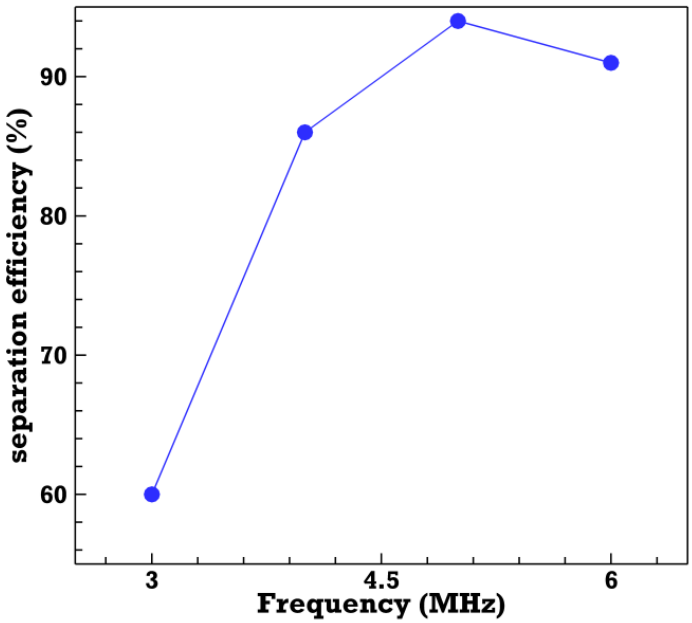

Fig. 9. Separation efficiency versus applied frequency when the mass flow rate is 0.2 ml/min and input power is 1.4 W.

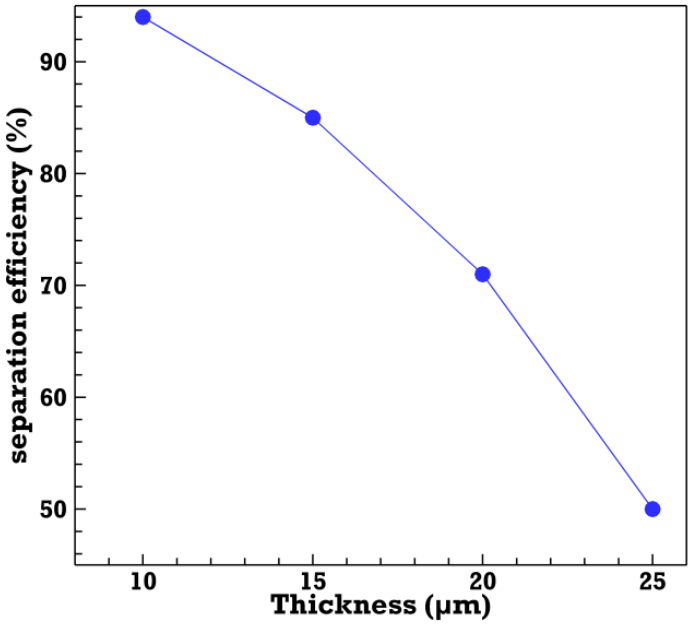

Fig. 10. Separation efficiency versus PDMS channel thickness when the inlet flow rate, frequency, and input power are 0.2 ml/min, 5 MHz, and 1.4 W, respectively.

5- 4- Effect of PDMS wall thickness

When the acoustic waves interact with the channel wall, they lose a part of their energy. Hence, the acoustic pressure is reduced as the PDMS channel thickness is enhanced. In other words, the location of pressure nodes and antinodes is changed when the channel thickness is varied. It has been demonstrated that the increment in the channel thickness intensifies the number of pressure nodes [4]. In this section, various channel thicknesses are considered to examine the separation efficiency when the inlet flow rate, frequency, and input power are 0.2 *ml/min*, 5 *MHz*, and 1.4 *W*, respectively. As expected, when the thickness of the microchannel wall is enhanced, the acoustic waves are more observed and the acoustic radiation force applied to the particles is reduced. Therefore, as shown in Fig. 10, the separation efficiency is reduced with the thickness of the microchannel wall.

6- Conclusions

The present work examines the separation of PS and PMMA particles by combining two passive and active methods in a microchannel that consists of spiral and straight sections. In the spiral part, passive separation occurs due to the rotation of the flow in the microchannel, and in the straight part, the sound field improves the separation efficiency. The results demonstrate that the separation efficiency is improved by increasing the frequency of the sound field and decreasing the inlet mass flow rate. It should be pointed out that there is an optimal value for the applied frequency due to the specific value of the channel width. Also, enhancing the input power increases the separation efficiency. As the distance between the transducers and the microchannel is enhanced, the separation efficiency is reduced. The proposed microchannel can separate up to 94% of the aforementioned particles, and since the influence of the acoustic field on biological samples is insignificant, this microfluidic device can be utilized to isolate biological cells. It is recommended to perform three-dimensional simulations to observe Dean vortices and their impact on the isolation of microparticles suspended in Newtonian and non-Newtonian fluids. Besides, an experimental approach can be employed to verify the findings.

References

[1] P. Sajeesh, A.K. Sen, Particle separation and sorting in microfluidic devices: a review, Microfluid Nanofluid, (17) (2014) 1–52.

[2] M. Bayareh, An updated review on particle separation in passive microfluidic devices, Chemical Engineering and Processing - Process Intensification, (153) (2020)107984.

[3] A. Shiriny, M. Bayareh, On magnetophoretic separation of blood cells using Halbach array of magnets. Meccanica, (55) (2020) 1903–1916.

[4] M. Nazemi Ashani, M. Bayareh, B. Ghasemi, Acoustofluidic separation of microparticles: a numerical study, Iranian Journal of Chemistry and Chemical Engineering, (41) (2022) 3064-3076.

[5] J.J. Stickel, R.L. Powell, Fluid mechanics and rheology of dense suspensions, Annu. Rev. Fluid Mech., (37) (2005) 129–49.

[6] O. Staufer, S. Antona, D. Zhang, J. Csatari, M. Schroter, J. W. Janiesch, S. Fabritz, I. Berger, I. Platzman, Microfluidic production and characterization of biofunctionalized giant unilamellar vesicles for targeted intracellular cargo delivery, Biomaterials, (264) (2021) 120203.

[7] Q. Li, S. Zhou, T. Zhang, B. Zheng, H. Tang, Bioinspired sensor chip for detection of miRNA-21 based on photonic crystals assisted cyclic enzymatic amplification method, Biosensors and Bioelectronics, (150) (2020) 111866.

[8] A. Lenshof, T. Laurell, Continuous separation of cells and particles in microfluidic systems, Chemical Society Reviews, (39) (2010) 1203-1217.

[9] A. Shiriny, M. Bayareh, Inertial focusing of CTCs in a novel spiral microchannel, Chemical Engineering Science, (229) (2020) 116102.

[10] A. Shiriny, M. Bayareh, a. Usefian, Inertial separation of microparticles suspended in shear-thinning fluids, Chemal Papers, (76) (2022) 4341–4350.

[11] J. Oakey, J. Allely, and D. W. Marr, Laminar-flow-based separations at the microscale, Biotechnology Progress, (18) (2002) 1439-1442.

[12] M. Yamada, M. Nakashima, M. Seki, Pinched flow fractionation: continuous size separation of particles utilizing a laminar flow profile in a pinched microchannel, Analytical Chemistry, (76) (2004) 5465-5471.

[13] J. Shi, H. Huang, Z. Stratton, Y. Huang, T. J. Huang, Continuous particle separation in a microfluidic channel via standing surface acoustic waves (SSAW), Lab on a Chip, (24) (2009) 3354–3359.

[14] P. Li, Z. Mao, Z. Peng, L. Zhou, Y. Chen, P.-H. Huang, Acoustic separation of circulating tumor cells, Proceedings of the National Academy of Sciences, (112) (2015) 4970-4975.

[15] H. M. Ji, V. Samper, Y. Chen, C. K. Heng, T. M. Lim, L. Yobas, Silicon-based microfilters for whole blood cell separation, Biomedical microdevices, (10) (2008) 251-257.

[16] C. W. Shields IV, C. D. Reyes, G. P. López, Microfluidic cell sorting: a review of the advances in the separation of cells from debulking to rare cell isolation, Lab on a Chip, (15) (2015) 1230-1249.

[17]] N. Nama, R. Barnkob, Z. Mao, C.J. Kähler, F. Costanzo, T.J. Huang Numerical study of acoustophoretic motion of particles in a PDMS microchannel driven by surface acoustic waves, Lab. Chip, 15 (12) (2015) 2700-2709.

[18] J.-C. Hsu, C.-H. Hsu, Y.-W. Huang, Acoustophoretic control of microparticle transport using dual-wavelength surface acoustic wave devices, Micromachines, 10 (1) (2019) 52.

[19] Z. Ma, D.J. Collins, Y. Ai, Single-actuator Bandpass Microparticle Filtration via Traveling Surface Acoustic Waves. Colloid and Interface Science Communications, (16) (2017) 6–9.

[20] J.L. Han, H. Hu, Q.Y. Huang, Y.L. Lei, Particle separation by standing surface acoustic waves inside a sessile droplet, Sensors and Actuators A: Physical, (326) (2021) 112731.

[21] T.D. Nguyen, Y.Q. Fu, V.T. Tran, A. Gautam, S. Pudasaini, H. Du, Acoustofluidic closed-loop control of microparticles and cells using standing surface acoustic waves, Sensors and Actuators B: Chemical, (318) (2020) 128143.

[22] J. Lei, F. Cheng, K. Li, Z. Guo, Numerical simulation of continuous separation of microparticles in two-stage acousto-microfluidic systems, Applied Mathematical Modelling, (83) (2020) 342-356.

[23] P.B. Muller, R. Barnkob, M. J. H. Jense, H. Bruus, A numerical study of microparticle acoustophoresis driven by acoustic radiation forces and streaming-induced drag forces, Lab on a Chip, (12) (2012) 4617-4627.

[24] F.J. Trujillo, P. Juliano, G. Barbosa-Canovas, K. Knoerzer, Separation of suspensions and emulsions via ultrasonic standing waves–A review, Ultrasonics Sonochemistry, (21) (2014) 2151–2164.

[25] F.J. Trujillo, S. Eberhardt, D. Möller, J. Dual, K. Knoerzer, Multiphysics modelling of the separation of suspended particles via frequency ramping of ultrasonic standing waves, Ultrasonics Sonochemistry, (20) (2013) 655–666.

[26] T. Franke, R.H.W. Hoppe, C. Linsenmann, L. Schmid, A. Wixforth, Optimal Control of Surface Acoustic Wave Actuated Sorting of Biological Cells, Trends in PDE Constrained Optimization. International Series of Numerical Mathematics, (165) (2014) 505-519.

[27] F. Petersson, A. Nilsson, C. Holm, H. Jonsson, T. Laurell, Separation of lipids from blood utilizing ultrasonic standing waves in microfluidic channels, The Royal Society of Chemistry, (129) (2004) 938-943.

HOW TO CITE THIS ARTICLE

Z. Taheri, M. Bayareh, B. Ghasemi, M. Nazemi Ashani, Simultaneous impacts of acoustic and inertial forces on the separation of microparticles , AUT J. Mech Eng., 7(1) (2023) 41-50.

DOI: 10.10.22060/ajme.2023.21665.6042/